International Journal of Microwave and Wireless Technologies

cambridge.org/mrf

Closed-form model to determine the co-axial probe reactance of an equilateral triangular patch antenna

Manotosh Biswas[1] and Mihir Dam[2]

[1]Department of Electronics & Tele-Communication Engineering, Jadavpur University, 188 Raja Subodh Chandra Mullick Road, Kolkata 700 032, India and [2]Department of Electronics, Vidyasagar College for Women, 39 Sankar Ghosh Lane, Kolkata 700 006, India

Research Paper

Cite this article: Biswas M, Dam M (2018). Closed-form model to determine the co-axial probe reactance of an equilateral triangular patch antenna. *International Journal of Microwave and Wireless Technologies* **10**, 801–813. https://doi.org/10.1017/S1759078718000661

Received: 4 October 2017
Revised: 29 March 2018
Accepted: 4 April 2018
First published online: 21 May 2018

Keywords:
Antenna design; input impedance; microwave measurements; modeling and measurements; probe reactance; quality factor; resonant frequency; triangular patch antenna

Author for correspondence:
Manotosh Biswas, E-mail: mbiswas@ieee.org

Abstract

A simple closed-form analytical formula is proposed to compute the probe reactance of an equilateral triangular patch antenna. The variation of the probe reactance with the variation of antenna dimension, substrate electrical parameters, and probe location is examined thoroughly. The computed values employing the present model show excellent agreement with experimental and simulation results.

Introduction

Since the quality factor (Q) of the triangular patch antenna is high [1], the antenna structure exhibits narrow band response. This inherent limitation of narrow band response of the triangular patch antenna might be a critical requirement for an antenna particularly to receive a narrow band signal in the presence of noise and can be utilized in designing of microstrip filters [2–5]. It is also being used to design microstrip compact array [6–8] with reduced coupling between adjacent elements. Recently, the triangular patch antennas are being used in designing microstrip sensors [9, 10], ring antennas [11, 12], reconfigurable [13], and multiple input and multiple output antennas [14]. It can also be used on curved surfaces because of its easy conformability.

The resonant frequency and the input impedance of triangular patch antenna have been investigated by several researchers [15–40] but those articles do not provide any information regarding the probe reactance. So, the works reported in [15–40] is insignificant for probe reactance computation of triangular patch antenna. The current paper is mainly focused on the investigation of probe reactance and its correct estimation. The coaxial probe feeding technique to a single microstrip element or arrays has become very popular and common in practice [41]. The probe reactance is highly sensitive to its location under the patch and it significantly affects the matching of input impedance [42, 43]. For a co-axial probe feeding technique, the outer conductor of the probe is connected with the ground plane of the antenna and the central conductor connected to the radiating patch by penetrating through the substrate as shown in Fig. 1 (a). The excitation of the patch principally occurs through the coupling of the probe current to the patch. The current through a central conductor of the probe creates surface electric current under the patch which produces the electric field. This field provides the probe reactance X_F is in series with the patch reactance itself. Therefore, the correct estimation of the probe reactance is very essential to match the input impedance between probe and patch properly.

In literatures, various numerical techniques e.g. Green's function [43–45], Mode matching [46], Vector Hankel Transform [47], etc. have been employed to analyze the probe reactance of rectangular and circular patch antenna yielding reasonably accurate results. But the numerical techniques are very complex, rigorous and time consuming in estimation of probe reactance. Harrington [48] developed a simple formula for the reactance of a current carrying probe within a parallel plate waveguide taking the source as a cylindrical wave function. Due to its simplicity, many researchers have used this formula to analyze the probe reactance. But a group of researchers [49] have reported that the computed probe reactance employing the Harrington's formula [48] does not match the measured reactance. In order to match the experimental and theoretical value of the probe reactance, an additional static capacitance was introduced in series with probe reactance [49]. This modified formulation shows better agreement near resonance at a specific probe location. In these works [48, 49], the effect of the probe location variation was not considered. Recently, Guha *et al.* [50] have modified the Harrington's formula [48] by multiplying it with the field factor to compute the probe reactance of rectangular and circular patch antenna. This model is suitable irrespective of operating frequency and feeds location under the patch. The works reported in [33, 36] are mainly focused on the computation of resonant frequency and input impedance. They have not considered the effect of probe reactance in input impedance computation. The work reported in [50] is focused

© Cambridge University Press and the European Microwave Association 2018

CAMBRIDGE UNIVERSITY PRESS

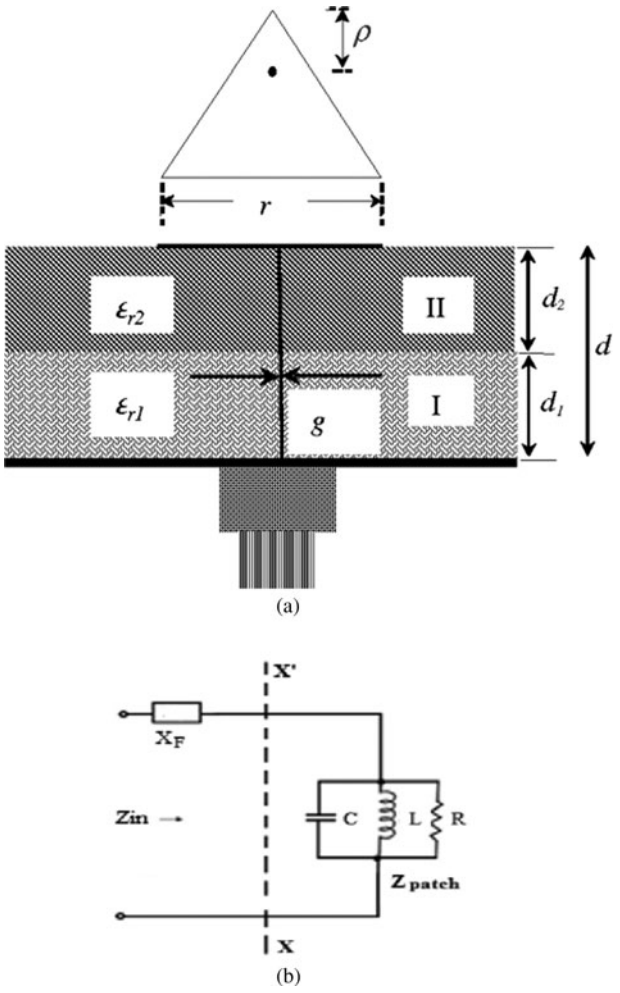


Fig. 1. (a) A schematic diagram of probe-fed equilateral triangular microstrip patch, (b) equivalent resonant parallel *R–L–C* circuits.

on rectangular and circular geometry. To the best of our knowledge, neither any design guideline nor any experimental results of the probe reactance of equilateral triangular patch antenna (ETPA) have yet been reported.

We, therefore, propose a very simple and efficient closed-form analytical formula to predict accurately the probe reactance of an ETPA. We have also proposed a set of closed-form expression to determine accurately the resonant frequency and input impedance of an ETPA. This efficient formula is capable to predict accurately the probe reactance for a wide variation of substrate electrical parameters. This formula also computes accurately the probe reactance as a function of frequency and probe location under the patch.

The expressions for this model are introduced in the "Theory" section. We have presented the predicted, measured and simulated results in the "Results and discussions" section. This section also includes the experimental test.

Theory

The probe reactance as a function of frequency may be obtained as [48]:

$$X_f(f) = \frac{\eta k_r d}{2\pi}\left[\ln\left(\frac{4}{kg}\right) - 0.577\right], \quad (1)$$

where g is the probe diameter, η is the intrinsic impedance of the medium, d is the thickness of the substrate, and k_r is the wave number. It is previously mentioned that probe reactance is highly sensitive to its location under the patch and it significantly influences the computation of input impedance. So the computation of probe reactance is incomplete until we incorporate the effect of probe feed location in it. The dependence of X_f on the location of the probe from the tip of the patch, defined as ρ in Fig. 1, can be derived as follows [50]:

Figure 1(b) shows an equivalent circuit of a probe-fed patch. Ideally, the patch itself can be looked upon from XX′ and this near resonance can be represented by a simple resistive network as shown in Fig. 2(a).

The quantity L_f is the probe inductance and $R(\rho)$ is the resonant resistance of the microstrip element which varies with ρ as:

$$R(\rho) = R_r P_{nml}(\rho), \quad (2)$$

$$P_{nml}(\rho) = (5\pi)^{-1}\left[\cos\frac{2\pi l\rho}{\sqrt{3}r} + \cos\frac{2\pi n\rho}{\sqrt{3}r} + \cos\frac{2\pi m\rho}{\sqrt{3}r}\right]^2, \quad (3)$$

where R_r is the resonant resistance of the patch. This circuit excited by an RF source will have the voltage–current relation as

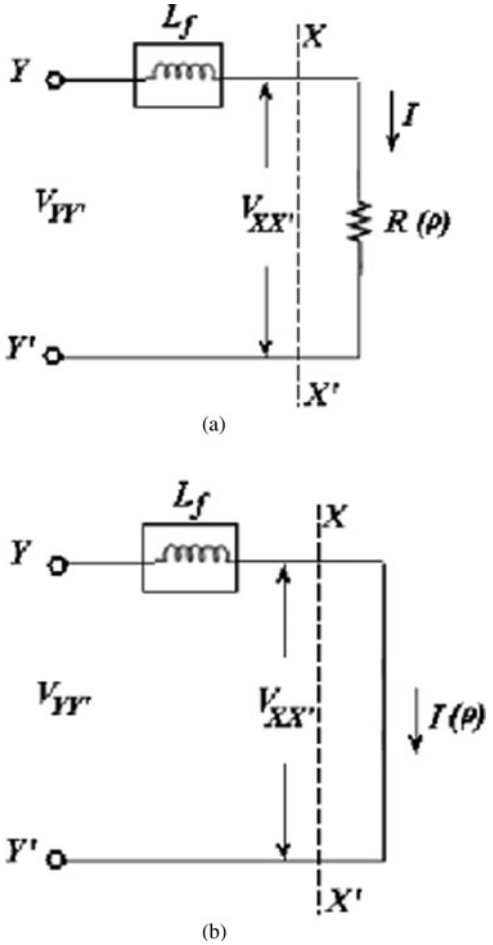


Fig. 2. Equivalent circuits for a microstrip patch fed by a coaxial probe. (a) Near resonance, (b) replacing $R(\rho)$ by $I(\rho)$ near resonance.

https://doi.org/10.1017/S1759078718000661 Published online by Cambridge University Press

$$V_{YY'} = L_f \frac{dI}{dt} + V_{XX'}, \tag{4}$$

where $V_{XX'}$ can be expressed for different ρ values as

$$V_{XX'} = I_{\rho 1} R(\rho_1) = I_{\rho 2} R(\rho_2). \tag{5}$$

Equation (5) implies that the product of $I(\rho)$ and $R(\rho)$ is constant and the profile of $I(\rho)$ and $R(\rho)$ is complementary to each other that is when $I(\rho)$ increases then $R(\rho)$ decreases or vice versa. So, $I(\rho)$ or $R(\rho)$ anyone can be replaced by other. So, the element $R(\rho)$ can be replaced by a branch current $I(\rho)$, which must follow the complementary profile of $R(\rho)$ [50]. Hence, for ETPA $I(\rho)$ may be represented as

$$I(\rho) = I_0 P'_{nml}, \tag{6}$$

$$P'_{nml}(\rho) = (5\pi)^{-1}\left[\cos \pi l\left(\frac{r/\sqrt{3}-\rho}{r}\right) + \cos \pi n\left(\frac{r/\sqrt{3}-\rho}{r}\right) + \cos \pi m\left(\frac{r/\sqrt{3}-\rho}{r}\right)\right]^2, \tag{7}$$

where I_0 is the current for $\rho = 0$.

When the element $R(\rho)$ is replaced by the branch current $I(\rho)$, then the equivalent circuit of Fig. 2(a) reduces to a reactive network as shown in Fig. 2(b) [50] and its terminal voltage can be written as

$$V_{YY'} = L_f \frac{dI(\rho)}{dt}. \tag{8}$$

This equation with the help of (6) reduces to

$$V_{YY'} = L_{f,e} \frac{dI_0}{dt}, \tag{9}$$

where $L_{f,e}$ is expressed as

$$L_{f,e} = L_f P'_{nml}(\rho). \tag{10}$$

Equation (10) finally determines the equivalent feed reactance which can account for its variation with the change in ρ. The relation (10) thus can be extended to modify Harrington's formula (1) as

$$X_f(f, \rho) = X_f(f) \times P'_{nml}(\rho). \tag{11}$$

This formula for probe reactance of an ETPA can be used for another triangular patch also. But only the appropriate field factors of the corresponding patch geometries are required.

The wave number k_r may be defined as

$$k_r = \frac{2\pi}{\lambda_{r,nml}} = \frac{2\pi f_{r,nml}}{c}, \tag{12}$$

where c is the velocity of light in free space and $f_{r,nml}$ is the resonant frequency. The accurate computation of resonant frequency is required due to accurate computation of probe reactance as a function of frequency. The $f_{r,nml}$ can be computed as [15]

$$f_{r,nml} = \frac{2c}{3r_{eff}\sqrt{\varepsilon_{r,\,eff}}}(n^2 + nm + m^2)^{1/2}, \tag{13}$$

where c is the velocity of light in free space, $\varepsilon_{r,eff}$ is the effective permittivity of the medium below the patch, r_{eff} is the effective side length of the patch and n, m, l are integers which are never zero simultaneously satisfying the condition $n + m + l = 0$.

In order to determine the r_{eff}, most of the researchers [15–30, 32, 35–40] assumed that all the modes have the same r_{eff}. But the different modes have the different fringing fields. The models reported in [31, 33–34] indicate that the r_{eff} is different for different modes. Thus, the mode dependent r_{eff} is computed from [34] as

$$r_{eff} = r(1 + \gamma q)^{1/2}. \tag{14}$$

In equation (14), q arises due to the fringing field at the edge of the patch and γ is the mode dependent factor. The model reported in [21] has been employed a curve fitting formula for computing r_{eff} and shows a large discrepancy between measured and computed values. Based on the concept employed in [21] we have proposed a curve-fitting formula for q based on experimental results [18, 21, 34] available in open literature and HFSS simulation results. This approach shows better agreement with the HFSS and experimental result. The q for this geometry is proposed as

$$q = q_1 + q_2 - q_3, \tag{15}$$

where

$$q_1 = 7.146\frac{d}{r} - 16.485\left(\frac{1}{\sqrt{\varepsilon_{re}}}\right)\left(\frac{d}{r}\right), \tag{16}$$

$$q_2 = 21.083\left(\frac{1}{\varepsilon_{re}}\right)\frac{d}{r} + 10.172\left(\frac{d}{r}\right)^2, \tag{17}$$

$$q_3 = 16.121\left(\frac{1}{\sqrt{\varepsilon_{re}}}\right)\left(\frac{d}{r}\right)^2, \tag{18}$$

where ε_{re} is the equivalent relative permittivity of the medium below the patch. The ε_{re} for a two-layer structure as shown in Fig. 1(a) may be defined as

$$\varepsilon_{re} = \frac{\varepsilon_{r1}\varepsilon_{r2}\, d}{\varepsilon_{r1} d_2 + \varepsilon_{r2}\, d_1}. \tag{19}$$

The fringing field is different for different operating modes of patch due to the field configuration [34] under the patch. In order to match the theoretical values with experimental values an empirical mode dependent factor was introduced in [34] in the expression of r_{eff}. In this paper, we have also incorporate an empirical mode dependent factor γ in the expression of r_{eff} for better matching between theoretical and experimental values as

$$\gamma = 0.75^m n^{0.23}, \tag{20}$$

here n and m are the mode indices.

Equation (14) in the present model and equation (6) in [34] are basically same. Here the fringing factor p of [34] has been

https://doi.org/10.1017/S1759078718000661 Published online by Cambridge University Press

replaced by q. In [34], p has been determined by equation (7) using the original expression of circular patch by employing an equivalence relation between circular and triangular geometry. In the present paper, we have proposed a new curve-fitting formula to compute q in equations (15)–(18) without employing any equivalence relation. Equation (8) in [34] and equation (20) in the present model are empirically proposed mode dependent factors to account the effect of modes in effective side length calculation.

In order to compute $\varepsilon_{r,eff}$ for a triangular patch, the triangular patch (side length r) is replaced by the rectangular patch (width W and length L) having an equivalent surface area. On the basis of an equivalence relation, we have

$$WL = (\sqrt{3}/4)r^2. \tag{21}$$

Now, we equate the zeroth-order resonant frequencies of a rectangular patch and triangular patch without fringing to get

$$f_{r,10,-1} = \frac{c}{2L\sqrt{\varepsilon_{re}}} = \frac{2c}{3r\sqrt{\varepsilon_{re}}}. \tag{22}$$

Thus,

$$L = (3/4)r. \tag{23}$$

The width (W) of the rectangular patch is obtained from (21) and (23) as

$$W = (1/\sqrt{3})r. \tag{24}$$

The $\varepsilon_{r,eff}$ for this structure is obtained from [51] as

$$\varepsilon_{r,eff} = \varepsilon_{re} - \frac{\varepsilon_{re} - \varepsilon_{r,dyn}}{1 + G(f_a/f_p)^2}, \tag{25}$$

where G is purely empirical term, $\varepsilon_{r,dyn}$ is the dynamic permittivity which depends on the dimensions, equivalent substrate relative permittivity ε_{re}, and field configurations of the mode under study [52], f_a is the frequency without fringing fields and ε_{re} is defined in (19). The G, f_a, and f_p are computed as

$$G = \sqrt{\frac{\varepsilon_{r,\,dyn}}{\varepsilon_{re}}}, \tag{26}$$

$$f_a = \frac{2c}{3r\sqrt{\varepsilon_{re}}}, \tag{27}$$

$$f_p = \frac{Z(r/d,\ d,\ \varepsilon_{re})}{2\mu_0 d} \tag{28}$$

$$Z\left(\frac{r}{d}, d, \varepsilon_{re}\right) = \frac{120\pi}{\sqrt{\varepsilon_{rf}(0)}}\left[\frac{r}{\sqrt{3}d} + 1.393 + 0.667\ln\left(\frac{r}{\sqrt{3}d} + 1.444\right)\right]^{-1}, \tag{29}$$

$$\varepsilon_{rf}(0) = \frac{\varepsilon_{re}+1}{2} + \frac{\varepsilon_{re}-1}{2}\left(1 + \frac{12d}{r/\sqrt{3}}\right)^{-1/2}. \tag{30}$$

The $\varepsilon_{r,dyn}$ for this structure is computed from [52] as

$$\varepsilon_{r,\,dyn} = \frac{C_{dyn}(\varepsilon = \varepsilon_0\varepsilon_{re})}{C_{dyn}(\varepsilon = \varepsilon_0)}, \tag{31}$$

where C_{dyn} (ε) is the total dynamic capacitance of the condenser formed by the conducting patch and the ground plane separated by a dielectric of permittivity ε. It takes into account the influence of the fringing field at the edge of the patch. The C_{dyn} (ε_0) is the total dynamic capacitance when $\varepsilon = \varepsilon_0$. The C_{dyn} (ε) can be written as

$$C_{dyn}(\varepsilon) = C_{0,dyn}(\varepsilon) + C_{e,dyn}(\varepsilon), \tag{32}$$

here $C_{e,dyn}$ (ε) and $C_{0,dyn}$ (ε) are the total dynamic fringe and main field capacitance respectively. The total dynamic fringe field capacitance $C_{e,dyn}$ (ε) for this structure is obtained from [52] as

$$C_{e,dyn}(\varepsilon) = \frac{1}{2}\left[\frac{Z(r/d,\, d,\, \varepsilon_{re} = 1)3r}{4cZ^2(r/d,\, d,\, \varepsilon_{re})} - C_{0,stat}(\varepsilon)\right]. \tag{33}$$

In (33), $C_{0,stat}$ is the static main field capacitance and may be obtained as

$$C_{0,stat}(\varepsilon) = \frac{\sqrt{3}\varepsilon_0\varepsilon_{re}r^2}{4d}. \tag{34}$$

The total dynamic main field capacitance $C_{0,dyn}$ (ε) is taken for the structure under study as [52]:

$$C_{0,dyn}(\varepsilon) = \gamma_{nm}C_{0,stat}(\varepsilon), \tag{35}$$

$\gamma_{nm} = 0.3525$, for $n = 1$; $\gamma_{nm} = 0.2865$, for $n = 2$; $\gamma_{nm} = 0.2865$, for $n = 3$.

The accurate computation of input impedance as a function of probe location is required for accurate computation of probe reactance as a function of probe location. The triangular geometry may be treated as a single resonant parallel R–L–C circuit as shown in Fig. 1(b). The input resistance and reactance seen by a coaxial probe located at a distance ρ from tip of the triangle may be computed as [34]:

$$R_{in} = \frac{R_r P_{nml}}{1 + Q_T^2\left[(f_{r,\,nml}/f) - (f/f_{r,\,nml})\right]^2}, \tag{36}$$

$$X_{in} = X_f(f, \rho) + \frac{R_r P_{nml} Q_T\left[(f_{r,\,nml}/f) - (f/f_{r,\,nml})\right]}{1 + Q_T^2\left[(f_{r,\,nml}/f) - (f/f_{r,\,nml})\right]^2}, \tag{37}$$

where R_r is the input resistance at resonance and it is different for different mode [20, 42–43], Q_T is the total quality factor, $f_{r,nml}$ is the mode depended resonant frequency is given by (13), f is the working frequency and P_{nml} is the field factor defined in (3). This is the very simple expression. But the large and rigorous mathematical steps have been employed in [20] for computing the R_{in} and X_{in}.

https://doi.org/10.1017/S1759078718000661 Published online by Cambridge University Press

Here we have employed a very simple and efficient expression to compute the mode-dependent R_r as provided in [40] as

$$R_r = \left[\frac{(0.18 + 0.83^n)}{m + 0.6^{nm}} - 1.6m(n-m)^2\right]\left(\frac{\eta d \lambda_{r,nm} \pi Q_T}{\alpha r^2 \sqrt{\varepsilon_{r,eff}}}\right). \quad (38)$$

The work reported in [20] has employed different mode dependent value for different modes for computing the input impedance. Here we have also introduced mode dependent factor for computing the input impedance. The first term indicates the mode-dependent factor. The factor α is a constant. The value of $\alpha = 7$ for right-angled isosceles triangular patch antenna [40] and for ETPA we have taken $\alpha = \sqrt{2}$. η is the intrinsic impedance of the medium, Q_T is the total quality factor, $\lambda_{r,nml} = c/f_{r,nml}$, $f_{r,nml}$ is the mode dependent resonant frequency is given by (13), $\varepsilon_{r,eff}$ is given by (25). n and m are the mode indices.

The Q_T consists of a quality factor due to radiation loss (Q_r), a quality factor due to dielectric loss (Q_d), and quality factor due to conductor loss (Q_c). The model reported in [20] has been employed rigorous and large mathematical steps for computing the different losses. But here we have proposed very simple formulas to compute the loss factors. The Q_T is defined as

$$Q_T = \left(\frac{1}{Q_r} + \frac{1}{Q_d} + \frac{1}{Q_c}\right)^{-1}. \quad (39)$$

The accurate computation of Q_r is very important because it determines the radiation efficiency. The computation of Q_r is very complex for triangular patch antenna due to its geometry. The Q_r depends on mode and field configuration under the mode [1]. Here we have taken a very simple and efficient expression to compute Q_r as proposed in [53, 54] and added a mode dependent correction factor. So, the final expression of Q_r as

$$Q_r = \left[\{2(n + 0.6nm) - 1\}^{0.6} - \frac{1.31(n-1)}{(n-0.6)}\right]\frac{\beta D(\delta)\varepsilon_{re}}{\mu_0 f_{r,nml} d}, \quad (40)$$

where the first term is the mode-dependent factor. The factor β is a constant. The value of $\beta = 21.15$ for circular patch antenna [53, 54] and we have employed $\beta = 30$ for ETPA. ε_{re} is defined in (19), $f_{r,nml}$ is given by (13), $D(\delta)$ is the directivity and n and m are the mode indices.

Here we have proposed a new curve fitting formula for computing the directivity of the structure under study based on simulation and experimental results as

$$D(\delta) = 3.194 - 0.482\delta + 3.042\delta^2 - 3.213\delta^3 + 4.924\delta^4 - 1.526\delta^5, \quad (41)$$

where

$$\delta = \frac{\pi f_{r,nml}}{2 f_{0,nml}\sqrt{\varepsilon_{re}}}, \quad (42)$$

and

$$f_{0,nml} = \frac{2c}{3r\sqrt{\varepsilon_{re}}}(n^2 + nm + m^2)^{1/2}. \quad (43)$$

The quality factor due to conductor loss Q_c, can be expressed as

$$Q_c = \frac{\pi\sqrt{\varepsilon_{r,eff}}}{\lambda_{r,nml}\,\alpha_c} \quad (44)$$

α_c is the conductor loss and obtained from [55] as

$$\alpha_c = \frac{R_s}{Z\left(\frac{r}{d}, d, \varepsilon_{re}\right) r/\sqrt{3}}, \quad (45)$$

$$R_s = \sqrt{\frac{\pi f_{r,nml}\mu_0}{\sigma}}, \quad (46)$$

where σ is the conductivity and other variables have usual meaning. Q_d for this structure can be computed as

$$Q_d = \frac{1}{\tan\,\delta_e}, \quad (47)$$

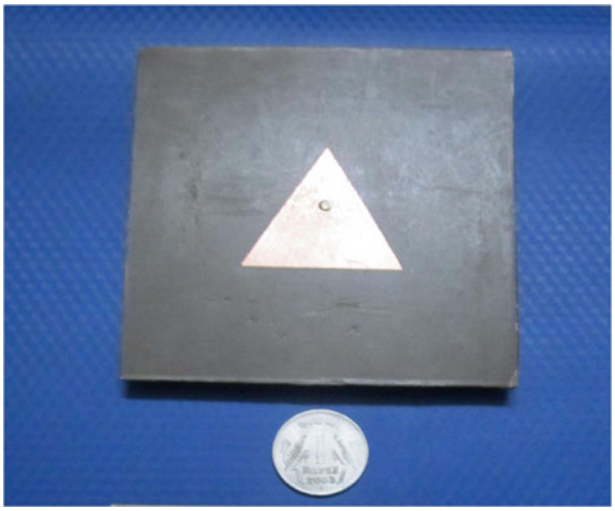


Fig. 3. Snapshot of a fabricated prototype of the tested antenna.

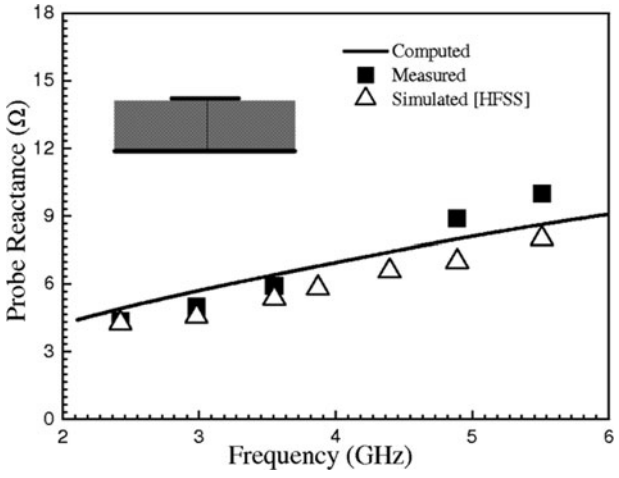


Fig. 4. Experimental, simulation and theoretical variation of probe reactance as a function frequency. $\varepsilon_{re} = \varepsilon_{r2} = 2.4$, $\tan\delta_e = \tan\delta_2 = 0.0022$, $d = d_2 = 0.8265$.

https://doi.org/10.1017/S1759078718000661 Published online by Cambridge University Press

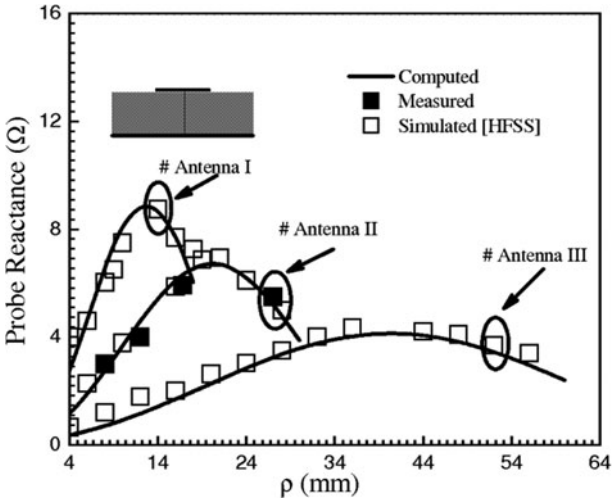


Fig. 5. Computed, measured and simulated variation of probe reactance as a function of probe location for different side length. $\varepsilon_{re} = \varepsilon_{r2} = 2.4$ $\tan\delta_e = \tan\delta_2 = 0.0022$, $d = d_2 = 0.8265$. # Antenna I ($r = 22$ mm); # Antenna II ($r = 35$ mm); # Antenna III ($r = 70$ mm).

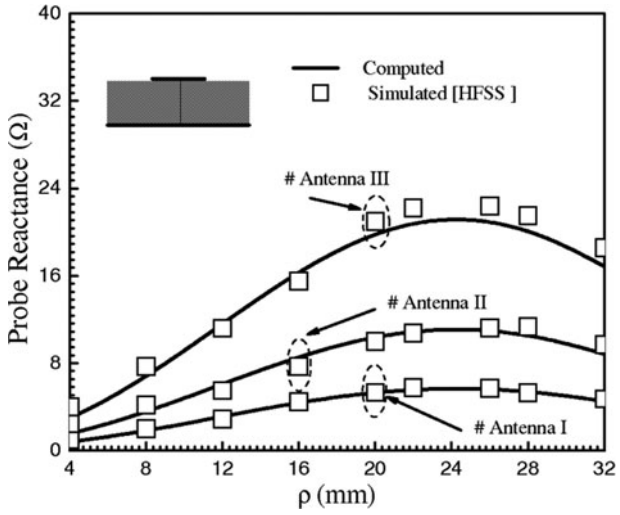


Fig. 7. Computed and simulated variation of probe reactance as a function probe location for different substrate thickness. $r = 42$ mm, $\varepsilon_{re} = \varepsilon_{r2} = 2.4$, $\tan\delta_e = \tan\delta_2 = 0.0022$. # Antenna I ($d = d_2 = 0.79$ mm); # Antenna II ($d = d_2 = 1.58$ mm); # Antenna III ($d = d_2 = 3.16$ mm).

where $\tan\delta_e$ is the equivalent loss tangent of a triangular patch on two dielectric layers may be defined as

$$\tan\delta_e = \frac{h_1\varepsilon_{r1}\tan\delta_1 + h_2\varepsilon_{r2}\tan\delta_2}{h\varepsilon_{re}}. \quad (48)$$

Results and discussions

Antenna design and experimental tests

A number of prototypes of different r has been etched on different substrates like (i) Rogers with $\varepsilon_{r2} = 2.4$, $d_2 = 0.8265$ and 1.58 mm, $\tan\delta_1 = 0.0022$; (ii) Glass epoxy with $\varepsilon_{r2} = 4.4$, $d_2 = 1.63$ mm, $\tan\delta_1 = 0.02$; and (iii) Arlon with $\varepsilon_{r2} = 10.0$, $d_2 = 1.63$ mm, $\tan\delta_1 = 0.0035$. One of the fabricated prototypes is shown in Fig. 3. The patch was excited with a coaxial probe whose diameter $g = 1.24$ mm. To validate the models developed in the "Theory" section, we have performed a series of experiments using Network Analyzer Agilent- E5071B. Here, we have presented the theoretically predicted, simulated, and measured results for the feed reactance, resonant frequency, and input impedance of an ETPA.

Probe reactance

In Fig. 4, we have compared the computed probe reactance X_f as a function of frequency employing the model with our experimental

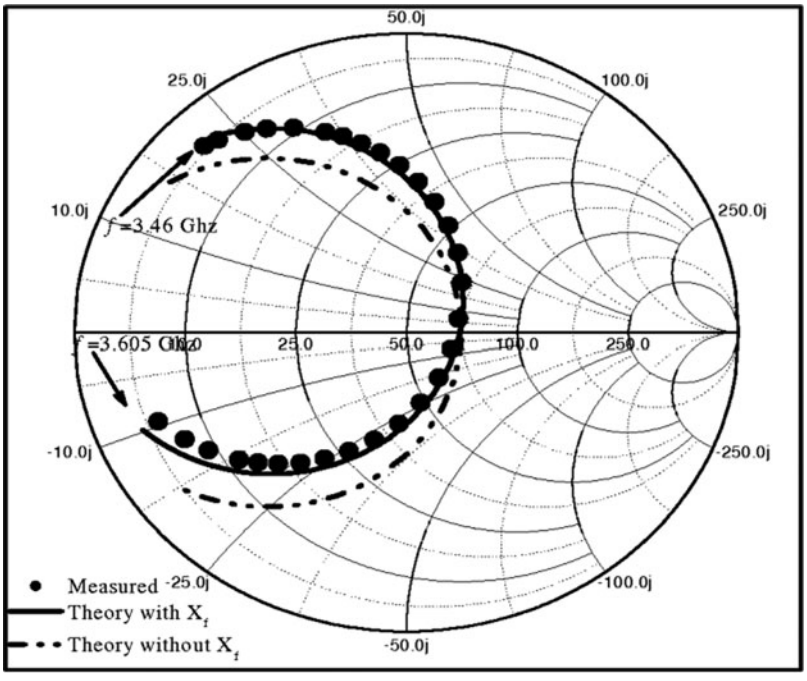


Fig. 6. Theoretical and experimental input impedance of an ETPA. $r = 35$ mm, $d = d_2 = 0.8265$, $\varepsilon_{re} = \varepsilon_{r2} = 2.4$, $\rho = 16.8$, $\tan\delta_e = \tan\delta_2 = 0.0022$.

https://doi.org/10.1017/S1759078718000661 Published online by Cambridge University Press

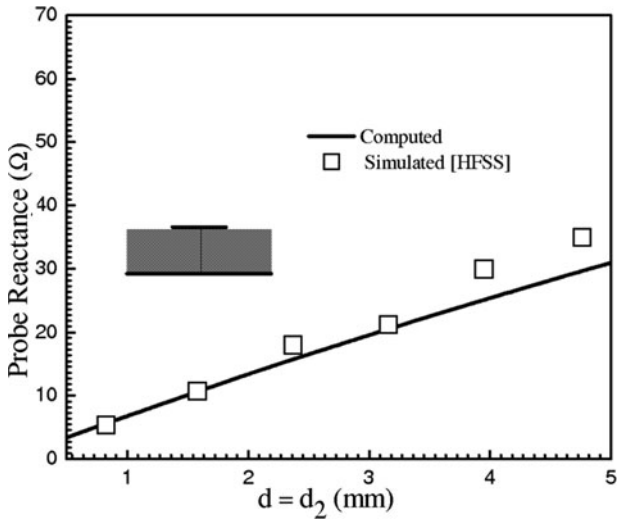


Fig. 8. Computed and simulated variation of probe reactance as a function substrate thickness. Parameters as in Fig. 7.

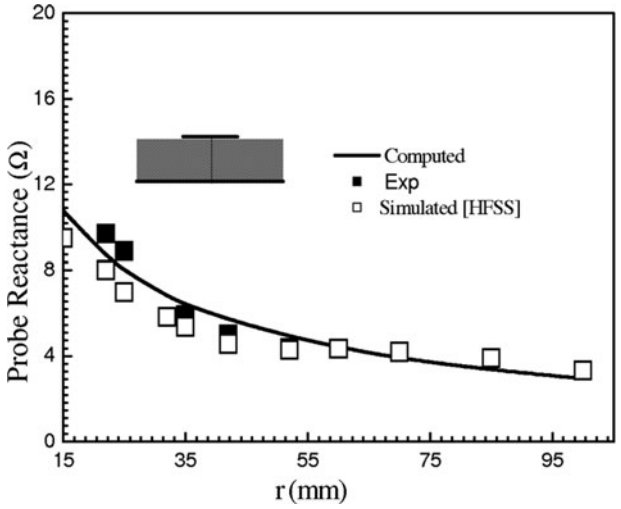


Fig. 11. Computed, simulated and measured variation of probe reactance as a function of side length r. $\varepsilon_{re} = \varepsilon_{r2} = 2.4$, $d = d_2 = 0.8265$ mm, $\tan\delta_e = \tan\delta_2 = 0.0022$.

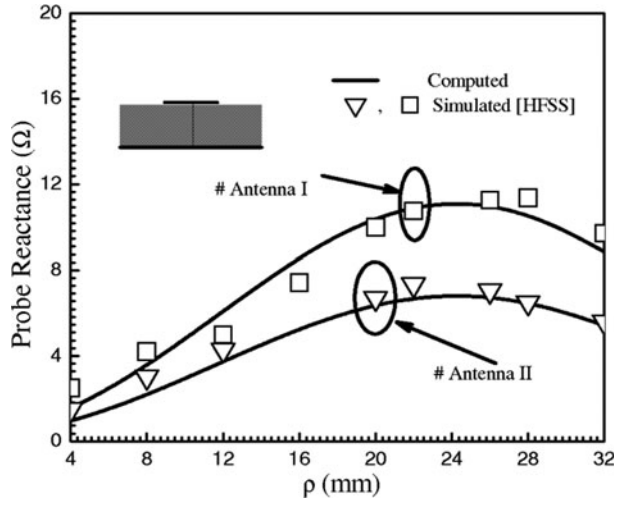


Fig. 9. Computed and simulated variation of probe reactance as a function feed location for different dielectric constant. $r = 42$ mm, $d = d_2 = 1.58$ mm, $\tan\delta_e = \tan\delta_2 = 0.0022$. # Antenna I ($\varepsilon_{re} = 2.4$); # Antenna II ($\varepsilon_{re} = 9.8$).

and simulation [56] results for an equilateral patch on single substrate and close agreement is revealed between them. The theoretical frequency is obtained by employing (13). The change in resonant frequency is obtained by changing side length r keeping all the antenna parameters unchanged. For each frequency, we have estimated the corresponding r. The 50 Ω probe location under the patch for every r is determined by employing (36). The probe reactance increases with the increase of frequency.

The variation of X_f as a function of probe position ρ for an equilateral patch on a single substrate having different r is depicted in Fig. 5. Here we have compared the computed X_f with simulation and our experimental results. The computed reactance curves well agree with the measured and simulated results. This study shows that the probe reactance increases with the decrease of r. When the side length r of the patch increases then the frequency of that patch decreases, as a result the probe reactance X_f decreases.

The effect of probe reactance X_f on input impedance is depicted in Fig. 6. Here measured input impedance is compared with the computed input impedance curve employing the

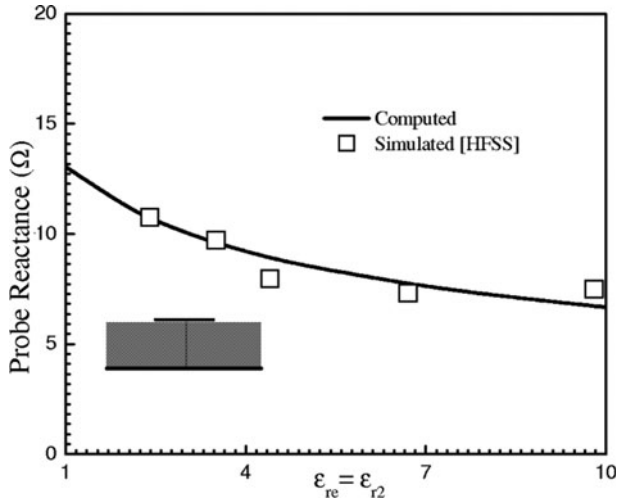


Fig. 10. Computed and simulated variation of probe reactance as a function of the dielectric constant of the substrate. Parameters as in Fig. 9.

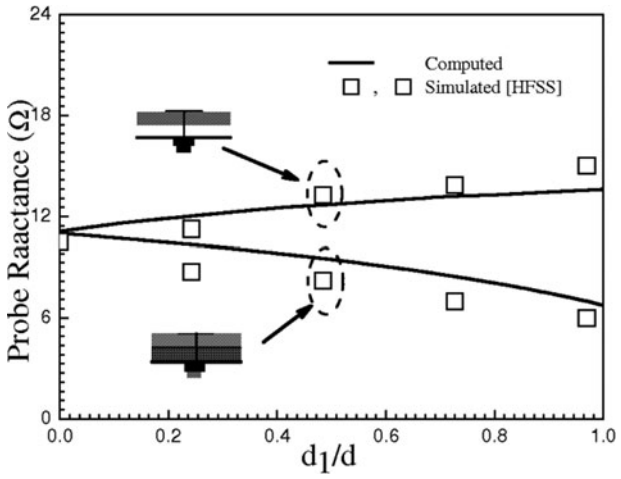
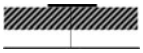


Fig. 12. Computed and simulated variation of probe reactance as a function of suspended ($\varepsilon_{r1} = 1.0$, $\tan\delta_1 = 0.000$) and composite ($\varepsilon_{r1} = 9.8$, $\tan\delta_1 = 0.0035$) substrate thickness. $r = 42$ mm, $\varepsilon_{r2} = 2.4$, $\tan\delta_2 = 0.0022$.

https://doi.org/10.1017/S1759078718000661 Published online by Cambridge University Press

Table 1. Theoretical, software computational, and experimental resonant frequencies for an equilateral triangular patch on two layers composite substrate operated in different modes. 

		Resonant frequency (GHz)						
					Computed			
d_1 (mm)	Mode	EXP.[I]	HFSS[II] [56]	CFDTD[III] [57]	Present	% Error with respect to [I]	% Error with respect to [II]	% Error with respect to [III]
0.8265	TM_{10}	2.427	2.393	2.389	2.388	1.607	0.209	0.042
	TM_{11}	4.316	4.247	4.233	4.247	1.599	0.000	−0.331
	TM_{20}	4.808	4.678	4.667	4.725	1.726	−1.005	−1.243
	TM_{21}	6.475	6.371	6.325	6.443	0.494	−1.130	−1.866
	TM_{30}	7.251	7.073	7.137	7.050	2.772	0.325	1.219
Average % error						1.639	0.534	0.939
1.58	TM_{10}	2.471	2.43	2.424	2.422	1.983	0.329	0.083
	TM_{11}	4.364	4.334	4.248	4.341	0.527	−0.162	−2.189
	TM_{20}	4.934	4.715	4.692	4.772	3.283	−1.209	−1.705
	TM_{21}	6.585	6.447	6.372	6.558	0.410	−1.722	−2.919
	TM_{30}	7.349	7.16	6.989	7.097	3.429	0.880	−1.545
Average % error						1.926	0.860	1.688
Total average % error						1.782	0.697	1.313
$r = 42$ mm, $\varepsilon_{r2} = 4.4$, $\varepsilon_{r1} = 2.4$, $d_2 = 1.63$								

Table 2. Theoretical, software computational and experimental resonant frequencies for an equilateral triangular patch on suspended substrate operated in different modes. 

		Resonant frequency (GHz)						
					Computed			
d_1 (mm)	Mode	EXP.[I]	HFSS[II] [56]	CFDTD[III] [57]	Present	% Error with respect to [I]	% Error with respect to [II]	% Error with respect to [III]
0.5	TM_{10}	3.495	3.435	3.452	3.477	0.515	−1.223	−0.724
	TM_{11}	6.189	6.09	6.143	6.169	0.323	−1.297	−0.423
	TM_{20}	7.002	6.86	6.913	6.863	1.985	−0.044	0.723
	TM_{21}	9.377	9.255	9.115	9.331	0.491	−0.821	−2.370
	TM_{30}	10.505	10.385	10.379	10.212	2.789	1.666	1.609
Average % error						1.221	1.010	1.169
1.0	TM_{10}	3.586	3.546	3.521	3.544	1.171	0.056	−0.653
	TM_{11}	6.206	6.275	6.162	6.354	−2.385	−1.259	−3.116
	TM_{20}	7.086	7.105	7.147	6.946	1.976	2.238	2.812
	TM_{21}	9.726	9.485	9.422	9.553	1.779	−0.717	−1.390
	TM_{30}	10.594	10.675	10.546	10.288	2.888	3.625	2.446
Average % error						2.039	1.579	2.083
Total average % error						1.63	1.294	1.626
$r = 42$ mm, $\varepsilon_{r2} = 2.4$, $\varepsilon_{r1} = 1.0$, $d_2 = 0.8265$								

https://doi.org/10.1017/S1759078718000661 Published online by Cambridge University Press

Table 3. Theoretical, software computational and experimental resonant frequencies for an equilateral triangular patch on single substrate operated in different modes.



Resonant frequency (GHz)										
							Computed			
r (mm)	$\varepsilon_{re}=\varepsilon_{r2}$	$d=d_2$ (mm)	Mode	EXP.[I]	HFSS[II] [56]	CFDTD[III] [57]	Present	% Error with respect to [I]	% Error with respect to [II]	% Error with respect to [III]
42	2.4	0.8265	TM_{10}	2.955	2.997	3.012	2.981	−0.880	0.534	1.029
			TM_{11}	5.225	5.117	5.289	5.225	0.000	−2.111	1.210
			TM_{20}	5.920	5.916	6.00	5.936	−0.270	−0.338	1.067
			TM_{21}	7.95	8.035	7.933	7.961	−0.138	0.921	−0.353
			TM_{30}	8.875	8.869	8.959	8.885	−0.113	−0.180	0.826
Average % error								0.280	0.817	0.897
42	4.4	1.63	TM_{10}	2.208	2.224	2.214	2.190	0.815	1.529	1.084
			TM_{11}	3.928	3.865	3.912	3.861	1.706	0.103	1.304
			TM_{20}	4.408	4.364	4.407	4.359	1.112	0.115	1.089
			TM_{21}	5.914	5.956	5.829	5.884	0.507	1.209	−0.944
			TM_{30}	6.609	6.446	6.547	6.526	1.256	−1.241	0.321
Average % error								1.079	0.839	0.948
42	10.0	1.63	TM_{10}	1.489	1.472	1.481	1.462	1.813	0.679	1.283
			TM_{11}	2.621	2.590	2.619	2.578	1.641	0.463	1.565
			TM_{20}	2.917	2.952	2.939	2.913	0.137	1.321	0.885
			TM_{21}	3.94	3.958	3.972	3.934	0.152	0.606	0.957
			TM_{30}	4.373	4.423	4.377	4.367	0.137	1.266	0.228
Average % error								0.776	0.867	0.938
22	2.4	0.8265	TM_{10}	5.587	5.505	5.478	5.513	1.325	−0.145	−0.639
			TM_{11}	9.829	9.725	9.822	9.753	0.773	−0.288	0.703
			TM_{20}	11.118	11.045	11.101	10.927	1.718	1.068	1.567
			TM_{21}	15.116	15.335	14.647	14.809	2.031	3.430	−1.106
			TM_{30}	16.435	16.140	16.393	16.310	0.761	−1.053	0.506
Average % error								1.321	1.197	0.904
Total Average % error								**0.864**	**0.930**	**0.922**

[I]Experiment.
[II]HFSS.
[III]CFDTD.

model with and without probe reactance. From this study, a discrepancy is observed between measured and computed input impedances when probe reactance X_f is not considered but the close agreement is seen between measured and computed input impedances when probe reactance X_f is considered.

In Fig. 7, authors present the variation of X_f as a function of probe location ρ under the patch for an equilateral patch on a single substrate having different substrate thickness d. Here we have compared the computed X_f with simulated [56] and close agreement is revealed between them.

The variation of X_f as a function of d for an equilateral patch is visualized in Fig. 8. In this study first we have determined the 50 Ω probe position under the patch for every d and then calculate the X_f. The X_f increases with increase of d. If the thickness of the substrate d increases, the length of the probe increases, the spurious radiation from the probe increases, the surface wave power increases and thus the probe reactance increases. Here the computed curve is compared with the HFSS simulated results. The slight discrepancy is observed for higher thickness. This is due to the fact that the Harrington's formula is well valid for small d/λ_0.

The variation of X_f with the variation of ρ for different ε_{re} of an equilateral patch on a single substrate is depicted in Fig. 9. In this study, we have compared the computed X_f curves with HFSS [53] simulation results. The computed curves well support the simulation results.

https://doi.org/10.1017/S1759078718000661 Published online by Cambridge University Press

Table 4. Theoretical and experimental values of resonant frequencies of an ETPA on single substrate operated in different.  $r = 100$ mm, $\varepsilon_{re} = \varepsilon_{r2} = 2.32$, $d = d_2 = 1.59$ mm, $\rho = 3$ mm.

Mode1	Resonant frequencies (GHz)								
		Computed							
	Measured [18]	Present	ALAIMAT [31]	CMA GA [24]	NASIM [28]	GUHA [27]	SDA MoM [21]	XG [19]
TM_{10}	1.280	1.280 (0.0)	1.286 (−0.469)	1.281 (−0.078)	1.283 (−0.234)	1.285 (−0.39)	1.288 (−0.63)	1.340 (−4.687)
TM_{11}	2.242	2.239 (0.134)	2.226 (0.714)	2.219 (1.025)	2.221 (0.936)	2.225 (0.76)	2.259 (−0.758)	2.320 (−3.479)
TM_{20}	2.550	2.550 (−0.0)	2.551 (−0.039)	2.562 (−0.470)	2.565 (−0.588)	2.570 (−0.784)	2.610 (−2.35)	2.679 (5.059)
TM_{21}	3.400	3.413 (−0.382)	3.400 (0.0)	3.389 (0.323)	3.393 (0.205)	3.400 (0.0)	3.454 (−1.59)	3.544 (−4.235)
TM_{30}	3.824	3.819 (0.131)	3.802 (0.575)	3.843 (−0.496)	3.848 (−0.627)	3.855 (−0.81)	3.875 (−1.33)	3.875 (−1.334)
Total average % Error		0.129	0.3594	0.478	0.518	0.5488	1.3316	3.759

In Fig. 10, we present the variation of X_f as a function of ε_{re}. The X_f decreases with the increase of ε_{re}. Here we have first estimated the 50 Ω probe position under the patch and then calculate the probe reactance. If the relative permittivity of the substrate ε_{re} increases, fringing field effect decreases, unwanted radiation from the probe decreases, and surface wave power decreases as a result the probe reactance decreases. The computed curve compared with the simulated curve and very close agreement is observed between them for all values of ε_{re}.

Figure 11 shows the variation of X_f as a function of r. The X_f decreases with the increase in r. The computed X_f is compared with simulated and our measured results. The close agreement is observed between them. Thus, the model is valid for a patch whose side length is varied from low to high value.

The effect of composite and suspended substrate on X_f is depicted in Fig. 12. For suspended substrate, the X_f is increased with the increase of d_1 whereas X_f decreases with the increase of d_1 for the composite substrate. The computed curves well support with the simulated results for all d_1/d. The effective permittivity for a composite substrate is enhanced, fringing field effect decreases, surface wave power decreases so the probe reactance decreases. The exactly opposite phenomena occur for the suspended substrate.

Now it is clear from the above studies in Figs 4–12 that X_f increase with the increase of thickness d and frequency f. X_f decreases with the decrease of side length r and relative permittivity ε_{re}. This information is very useful for practical implementation of the ETPA.

Validity of resonant frequency

In Table 1, we have compared the computed resonant frequencies employing the present model with simulation [56, 57] and our experimental results for an equilateral patch on two dielectric layers operated in dominant and higher order modes. The total average error of the present model is computed against the simulated and measured results. The total average % errors are 1.782, 0.697, and 1.313 against experimental, HFSS, and CFDTD simulation results, respectively. From this comparison we observe that

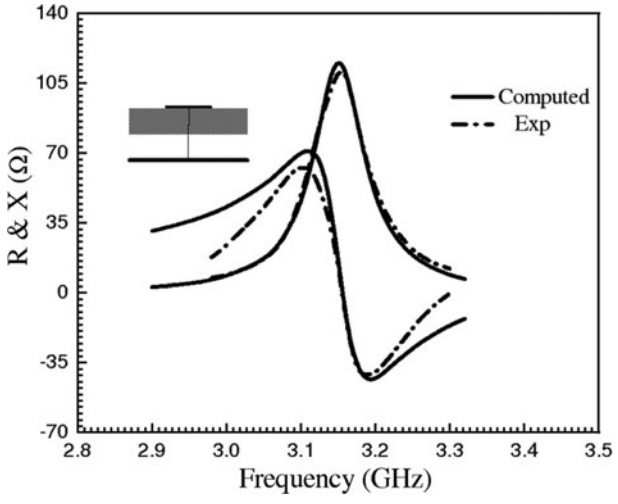


Fig. 13. Measured and computed dominant mode input impedance as a function of frequency for a probe-fed equilateral triangular patch on suspended substrate having $d_1 = 0.45$ mm $d_2 = 1.58$ mm, $r = 42$ mm, $\varepsilon_{r1} = 1.0$, $\varepsilon_{r2} = 2.4$, $\tan\delta_1 = 0.0$, $\tan\delta_2 = 0.0022$, $\rho = 19.20$ mm.

https://doi.org/10.1017/S1759078718000661 Published online by Cambridge University Press

Table 5. Experimental theoretical values of resonant frequency and input impedance of an ETPA on single substrate operated in different modes. $r = 100$ mm, $\varepsilon_{r2} = 2.32$, $d = d_2 = 1.59$, $\rho = 3.0$ mm.



	Resonant frequency (GHz)			Input impedance (Ω)		
		Theory			Theory	
Mode	Measured [20]	Lee [20]	Present	Measured [20]	Lee [20]	Present
TM_{10}	1.280	1.299	1.280	1510	1640	1509
TM_{20}	2.550	2.599	2.550	340	450	367
TM_{21}	3.400	3.439	3.413	949	909	933
Total % average error		1.519	0.127	Total % average error	15.059	3.231

the error in the model against experimental results is slightly high. This is due to the fact that a tiny air gap may be present between two dielectric layers and this cannot be avoided.

A comparison of simulated [56, 57] and our measured resonant frequencies with computed values for an equilateral patch on suspended substrate operated in dominant and higher order modes is presented in Table 2. The total average percentage errors are 1.63, 1.294, and 1.626 against experimental, HFSS, and CFDTD simulation results, respectively.

In Table 3, we compare the computed resonant frequencies employing the model with simulated and our measured results for an equilateral patch printed on a single substrate operated in dominant and higher order modes. The total average percentage errors are 0.864, 0.930, and 0.922 against experimental, HFSS, and CFDTD simulation results, respectively.

From Tables 1–3, we conclude that the present model very accurately computed the resonant frequencies against HFSS, CFDTD simulation, and our experimental results.

Now the accuracy of the present model is verified against the other measured results [18] in Table 4. Here the measured resonant frequencies obtained from [18] are compared with different theoretical models reported in [19, 21, 24, 27, 28, 31] and in this work for an equilateral patch printed on a low dielectric constant substrate operated in dominant and higher order modes. This comparison shows that present model more accurately computed the resonant frequencies.

From the above comparison in Tables 1–4 it is clear that the present formulae based on cavity model are valid for a wide variation of substrate permittivity; patch side length and substrate thickness. But the slight discrepancy is observed for a patch having very smaller side length or larger substrate thickness. Because the accuracy of the present model mainly depends on the value of h/λ_0 and it is well suitable for a small value of h/λ_0. This is not the limitation of the present model but it is the inherent limitation of the cavity model.

Validity of input impedance

A comparison of theoretically predicted input impedance with our measured results for an equilateral patch printed on a suspended substrate is depicted in Fig. 13. The computed curve for input impedance is close to the measured results.

The accuracy of the model is further verified with other measured results [20] in Table 5. Here we compare the computed input impedance employing the present model and model reported in [20] with experimental results [20] for an equilateral triangular patch operated in dominant and higher order modes. Here we consider an equilateral patch having side length $r = 100$ mm printed on a substrate whose $d = 1.59$ mm, $\varepsilon_{re} = 2.32$, $\tan\delta_e = 0.0005$, $d/\lambda_r = 0.0068$ and probe is located as a distance $\rho = 3.0$ mm from the tip of the triangle. The present model shows very less error compared to the model reported in [20].

Conclusion

The radiated power and impedance bandwidth of an ETPA mainly controlled by the input impedance. For probe-fed patch antenna, the total input impedance consists of the probe reactance in series with the patch impedance. Good models for calculating patch impedance are available, but to the best of our knowledge no model is available to compute probe reactance of an ETPA. For the first time, a very simple and efficient formula is proposed to accurately predict the probe reactance of an ETPA. To overcome the drawback of earlier models as discussed detail in the "Introduction" section, we have introduced the field factor in the Harrington's formula. This efficient formula is capable of predicting accurately the probe reactance for a wide variation of substrate electrical parameters, antenna dimension, and probe position under the patch. Present theoretical analysis shows excellent agreement with our measured results. We have also employed electromagnetic software to validate the model.

References

1. **Garg R *et al.*** (2001) *Microstrip Antenna Design Handbook*. Artech House.
2. **Liu Q, Wang J and He Y** (2017) Compact balanced band pass filter using isosceles right triangular patch resonator. *Electronics Letters* **53**, 253–254.
3. **Yadav S *et al.*** (2016) Design of band-rejected UWB planar antenna with integrated Bluetooth band. *IET Microwaves, Antennas and Propagation* **10**, 1528–1533.
4. **Liu HW, Cheng ZQ and Sun LL** (2006) Dual-mode triangular-patch band pass filter using spur-lines. *Electronics Letters* **42**, 762–763.
5. **Hong J-S and Lancaster MJ** (2004) Theory and experiment of dual-mode microstrip triangular patch resonators and filters. *IEEE Transactions on Microwave Theory and Techniques* **52**, 1237–1243.
6. **Luo Q *et al.*** (2016) Dual circularly polarized equilateral triangular patch array. *IEEE Transactions on Antennas and Propagation* **64**, 2255–2262.
7. **Sumantyo JTS and Ito K** (2006) Circularly polarized equilateral triangular patch array antenna for mobile satellite communications. *IEE Proceedings – Microwaves, Antennas and Propagation* **153**, 544–550.
8. **Sumantyo JTS, Ito K and Takahashi M** (2005) Dual-band circularly polarized equilateral triangular-patch array antenna for mobile satellite communications. *IEEE Transactions on Antennas and Propagation* **53**, 3477–3485.
9. **Biswas M and Mandal A** (2014) Design and development of an equilateral patch sensor for determination of permittivity of homogeneous

https://doi.org/10.1017/S1759078718000661 Published online by Cambridge University Press

dielectric medium. *Microwave and Optical Technology Letters* **56**, 1097–1104.
10. **Jobs M and Rydberg A** (2012) Conformal dual patch antenna for diversity based sensor nodes. *Electronics Letters* **48**, 306–307.
11. **Zhang T *et al.*** (2014) Triangular ring antennas for dual-frequency dual-polarization or circular-polarization operations. *IEEE Antennas and Wireless Propagation Letters* **13**, 971–974.
12. **Chen J-S** (2005) Studies of CPW-fed equilateral triangular-ring slot antennas and triangular-ring slot coupled patch antennas. *IEEE Transactions on Antennas and Propagation* **53**, 2208–2211.
13. **Sung Y** (2010) Investigation into the polarization of asymmetrical-feed triangular microstrip antennas and its application to reconfigurable antennas. *IEEE Transactions on Antennas and Propagation* **58**, 1039–1046.
14. **Zhang H *et al.*** (2008) A compact MIMO antenna for wireless communication. *IEEE Antennas and Propagation Magazine* **50**, 104–107.
15. **Helszajn J and James DS** (1978) Planar triangular resonators with magnetic walls. *IEEE Transactions on Microwave Theory and Techniques* **26**, 95–100.
16. **Sharma AK and Bhat B** (1982) Analysis of triangular microstrip resonator. *IEEE Transactions on Microwave Theory and Techniques* **30**, 2029–2031.
17. **Keuster EF and Chang DC** (1983) A geometrical theory for the resonant frequencies and Q factors of some triangular microstrip patch antennas. *IEEE Transactions on Antennas and Propagation* **31**, 27–34.
18. **Dahele JS and Lee KF** (1987) On the resonant frequencies of the triangular patch antenna. *IEEE Transactions on Antennas and Propagation* **35**, 100–101.
19. **Gang X** (1989) On the resonant frequencies of microstrip antennas. *IEEE Transactions on Antennas and Propagation* **37**, 245–247.
20. **Lee KF, Luk KM and Dahele JS** (1988) Characteristics of the equilateral triangular patch antenna. *IEEE Transactions on Antennas and Propagation* **36**, 1510–1518.
21. **Chen W, Lee KF and Dahele JS** (1992) Theoretical and experimental studies of the resonant frequencies of equilateral triangular microstrip antenna. *IEEE Transactions on Antennas and Propagation* **40**, 1253–1256.
22. **Hassani HR and Mirshekar Syahkal D** (1992) Analysis of triangular patch antennas including radome effects. *IEE Proceedings H* **139**, 251–256.
23. **Biswas M and Dam M** (2018) CAD oriented improved cavity model to investigate a 30°–60°–90° right angled triangular patch antenna on single, composite and suspended substrate for the application in portable wireless equipments. *IET Microwaves, Antennas & Propagation* **12**, 425–434.
24. **Karaboğa D *et al.*** (1997) Simple and accurate effective side length expression obtained by using a modified genetic algorithm for the resonant frequency of an equilateral triangular microstrip antenna. *International Journal of Electronics* **83**, 99–108.
25. **Gurel CS and Yazgan E** (2000) New computation of the resonant frequency of a tunable equilateral triangular microstrip patch. *IEEE Transactions on Microwave Theory and Techniques* **48**, 334–338.
26. **Lim EG *et al.*** (2002) An efficient formula for the input impedance of a microstrip right-angled isosceles triangular patch Antenna. *IEEE Antennas and Wireless Propagation Letters* **1,** 18–21.
27. **Guha D and Siddiqui JY** (2004) Resonant frequency of equilateral triangular microstrip patch antenna with and without air gaps. *IEEE Transactions on Antennas and Propagation* **52**, 2174–2177.
28. **Nasimuddin KE and Verma AK** (2005) Resonant frequency of an equilateral triangular microstrip antenna. *Microwave and Optical Technology Letters* **47**, 485–489.
29. **Biswas M and Guha D** (2009) Input impedance and resonance characteristic of superstrate loaded triangular microstrip patch. *IET Microwaves, Antennas & Propagation* **3**, 92–98.
30. **Biswas M and Mandal A** (2010) CAD model to compute the input impedance of an equilateral triangular microstrip patch antenna with radome. *Progress in Electromagnetics Research M* **12**, 247–257.
31. **Olaimat MM and Dib NI** (2011) Improved formulae for the resonant frequencies of triangular microstrip patch antennas. *International Journal of Electronics* **98**, 407–424.
32. **Olaimat MM and Dib NI** (2011) A study of 15°–75°–90° angles triangular patch antenna. *Progress in Electromagnetics Research Letters* **21**, 1–9.
33. **Biswas M and Dam M** (2012) Fast and accurate model of equilateral triangular patch antennas with and without suspended substrates. *Microwave and Optical Technology Letters* **54**, 2663–2668.
34. **Biswas M and Dam M** (2013) Theoretical and experimental studies on characteristics of an equilateral triangular patch antenna with and without variable air. *Microwave and Optical Technology Letters* **55**, 2271–2277.
35. **Maity S and Gupta B** (2013) Simplified analysis for 30°–60°–90° triangular microstrip antenna. *Journal of Electromagnetic Waves and Applications* **28**, 91–101.
36. **Maity S and Gupta B** (2013) Accurate resonant frequency of isosceles right-angled triangular patch antenna. *Microwave and Optical Technology Letters* **55**, 1306–1308.
37. **Maity S and Gupta B** (2015) Cavity model analysis of 30°–60°–90° triangular microstrip antenna. *AEU – International Journal of Electronics and Communications* **69**, 923–932.
38. **Guney K and Erhan K** (2016) Effective side length formula for resonant frequency of equilateral triangular microstrip antenna. *International Journal of Electronics* **103**, 261–268.
39. **Maity S and Gupta B** (2017) Approximate investigation on isosceles triangular microstrip antenna in fundamental mode. *Microwave and Optical Technology Letters* **59**, 614–618.
40. **Dam M and Biswas M** (2017) Investigation of a right-angled isosceles triangular patch antenna on composite and suspended substrates based on a CAD-oriented cavity model. *IETE Journal of Research* **63**, 248–259.
41. **Lee KF and Chen W** (1997) *Advances in Microstrip and Printed Antennas*. New York: Wiley.
42. **Richards WF, Lo YT and Harrison DD** (1981) An improved theory for microstrip antennas and applications. *IEEE Transactions on Antennas and Propagation* **29**, 38–46.
43. **Yano S and Ishimaru A** (1981) A theoretical study of the input impedance of a circular microstrip disk antenna. *IEEE Transactions on Antennas and Propagation* **29**, 77–83.
44. **Chen W, Lee KF and Lee RQ** (1993) Input impedance of coaxially fed rectangular microstrip antena on electrically thick substrate. *Microwave and Optical Technology Letters* **6**, 387–390.
45. **Aberle JT, Pozar DM and Birtcher CR** (1991) Evaluation of input impedance and radar cross section of probe-fed microstrip patch elements using an accurate feed model. *IEEE Transactions on Antennas and Propagation* **39**, 1691–1696.
46. **Davidovitz MY and Lo T** (1986) Input impedance of a probe-fed circular microstrip antenna with thick substrate. *IEEE Transactions on Antennas and Propagation* **34**, 905–911.
47. **Chew WC and Kong JA** (1981) Analysis of a circular microstrip disk antenna with a thick dielectric substrate. *IEEE Transactions on Antennas and Propagation* **29**, 68–76.
48. **Harrington RF** (1961) *Time-Harmonic Electromagnetic Fields*. New York: McGraw-Hill, p. 228.
49. **Alarjani BM and Dahele JS** (2000) Feed reactance of rectangular microstrip patch antenna with probe feed. *Electronics Letters* **36**, 388–390.
50. **Guha D, Biswas M and Siddiqui JY** (2007) Harrington's formula extended to determine accurate feed reactance of probe-fed microstrip patches. *IEEE Antennas and Wireless Propagation Letters* **6**, 33–35.
51. **Edwards TC and Steer MB** (2000) *Foundations of Interconnect and Microstrip Design*, 3rd Edn. USA: John Wiley & Sons Ltd.
52. **Wolff I and Knoppik N** (1974) Rectangular and circular microstrip disk capacitors and resonators. *IEEE Transactions on Microwave Theory and Techniques* **22**, 857–864.
53. **Abboud F, Damiano JP and Papiernik A** (1990) A new model for calculating the input impedance of coax-fed circular microstrip antennas with and without air gaps. *IEEE Transactions on Antennas and Propagation* **38**, 1882–1885.
54. **Derneryd AG** (1979) Analysis of the microstrip disk antenna element. *IEEE Transactions on Antennas and Propagation* **27**, 660–664.
55. **Pozar DM** (2012) *Microwave Engineering*, 4th Edn. USA: John Wiley & Sons, Inc.
56. **Ansoft Corp.** (2012) *High Frequency Structure Simulator*.
57. **Mittra R and Yu W** (2004) *CFDTD*. Artech House.

https://doi.org/10.1017/S1759078718000661 Published online by Cambridge University Press



Manotosh Biswas was born in West Bengal, India, in 1976. He received his B.Tech., M.Tech., and Ph.D. degrees in Radiophysics and Electronics from the University of Calcutta, India, in 2001, 2003, and 2008, respectively. Dr Biswas obtained the Young Scientist Award from URSI in 2005 and is a senior member of IEEE. He started his carrier in the Department of Electronics, West Bengal State University, India as a Reader in February 2009. In July 2010, he joined as a Reader in the Department of Electronics & Tele-Communication Engineering, Jadavpur University, India and currently he is serving as an Associate Professor at the same University. His research interest includes Planner Antennas, Dielectric Resonator Antennas, and metamaterials. He has published more than 26 technical journal articles and 50 technical conference proceedings articles.



Mihir Dam was born in Kolkata, India, on January 1, 1983. He received the M.Sc. degree in Electronic Science in 2006 and the M.Tech. degree in Radiophysics and Electronics in 2007 from Calcutta University, India. He is currently working toward the Ph.D. degree at Jadavpur University in the field of Microstrip patch antennas. At the same time, he is also working as an Assistant Professor in the Department of Electronics, Vidyasagar College for Women. He has published more than five technical journals and more than 14 technical conference articles.

https://doi.org/10.1017/S1759078718000661 Published online by Cambridge University Press